Exploring Bandgap Engineering on Photovoltaics and their Possible Economic implications

Exploring Bandgap Engineering on Photovoltaics and their Possible Economic implications

T.J. Abodunrin [1*], M.E. Emetere [1] , O.O. Ajayi [2] A.P.I. Popoola [3], O. Popoola [4] and U. O. Uyor [3]

,
[1] Department of Physics, Covenant University, Ota, Ogun State, Nigeria.
[2] Department of Mechanical Engineering, Covenant University, Ota, Ogun State, Nigeria.
[3]Department of Chemical, Metallurgical and Materials Engineering, Tshwane University of Technology, South Africa.
Corresponding Author; temitope.abodunrin@covenantuniversity.edu.ng, +2347030380040

Abstract-
Bandgap an intrinsic property of molecules on nanoscale, has capability of making alterations in the characteristics of the material through cataclysmic changes from interaction with light. Ultraviolet spectrographs of three organic extracts were explored for their optical frequency and possible use as communication organic optical fiber. The bandgaps of these dye extracts were determined and tailored by varying their absorptivity of ions in electrolytic solvents. A distinctive absorption power, transmittance and amplitude promoted vital regional shifts in wavelength. Interaction with radiation absorbed, influenced a Fermi energy change within a large band gap ≈ 4eV, which is a hypothetical line of symmetry. Results revealed that all the bands below that energy level were entirely filled, whereas all higher-lying bands were completely or nearly empty, with the exception of minimal thermal excitation which is induced at high temperatures.

Key words: Organic optical fiber, Bandgap, transmittance, frequency

1. Introduction

Band gap is fundamental to photovoltaics and other applications [1]. Organic molecules, semiconductors, metals and dielectric substances have direct band gap; a low band gap is characterized by strong absorbance in the visible region of the electromagnetic spectrum [2]. In broad terms, high absorbance coefficients reveal a band gap value within the range of 1.55 eV [3]. Band gap can be modified by regulation of the geometry of material substances, this is usually accomplished by varying temperature and/or interchanging components of matter [4]. A little decrease in the band gap such as 0.06 eV can be obtained by a decrease in temperature of 150 K [5].
In stoichiometry, replacement of any organic cations not only affect the electronic structure directly but changes the entire geometry of the skeletal frame. Equilibrium is attained through the organic cations' regulation of their bond distance between neighboring atoms in a bid to identify the easiest route for charge transport [6]. Myriads of band gap researches has evolved ferroelectric materials, complex oxides, heterogenous and anisotropic monolayer phases [7].

Investigation of size and shape of organic cations ultimately resulted in cladding of rare-earth organic complexes to eliminate limitations associated with junction losses in most waveguide structures. More progressive research resulted in the incorporation of optical properties of rare-earth organic complexes in polymer optical fibers and waveguides [8]. Consequently, Er^{3+}, Nd^{3+}, and Sm^{3+} were encapsulated in organic chelates and their radiative properties.

Analysis reveals that chelates are prospective choices for dopant use in rare-earth-doped polymer devices [9]. A unique feature is that, rare-earth complexes enable short-length amplification in devices doped to high concentrations without quenching [10]. A limitation to their universal adoption lies in their scarcity and high cost of most rare-earth elements [11]. However, nano dimension optical fibers employ Layer by Layer deposition techniques which work independently of morphology and size of the substrate [12]. This makes feasible the use of substitutes, attributable to sequence of procedures, generating matrixes on diverse substrates at a molecular level [13].

The resultant effect is photonic bandgap formation by synergistic interplay between two distinct resonance scattering mechanisms [14]. Thus, this work aims at utilizing electrostatic attraction of organic dye molecules, to explore ionic nature groups in solvents for possible applications in optical fiber telecommunications within the UV-Vis frequency [15].

2. Experimental Methods

Dye culture of three leaf extracts were cultured from 1g dye dissolved in 100 ml deionized water for 24 h. Consequently, the extracts from Butternut (*C. moschata*), Ringwood (*S. anisatum*), Beetroot (*B. vulgaris*) and African Star Apple (*C. albidum*) were each affixed as monolayer onto indium doped tin oxide (ITO) conducting glasses, to increase the initial thickness. A second ITO had three monolayers of Pt deposited to vary the reflected power [14-15]. Illuminating sensors from UV/Vis spectrophotometer generated signals at different wavelengths in absorbance units for each of the dye. The thickness of each individual layer on nanometric scale, was interrogated by beams from the scanning electron microscope which produced images of the microstructure of each sample by scanning the surface with a light probe comprising of a focused beam of electrons. The electrons interacted with atoms in the dye samples, producing various signals equivalent to that of a multiplexer optical channel delivering information on composition and surface topography and of the dyes. The laser was tuned to the wavelength of one of the chromophores, this signal from the sensor was recorded. Then, the laser tuned to another chromophore at another wavelength, the sensor noted it, as a channel wavelength [16].

3. Results and discussion

UV/Vis Spectroscopy: In this study, UV–Vis spectrographs were employed as a direct method for determining precise estimate of the band gap energy of four organic π-conjugated materials. The energy transitions inside the material were recognized by ultraviolet spectroscopy. The connection between dye concentration and the optical path length is referred to absorption (A) which is otherwise known as, the optical density. This is as illustrated by Beer Lambert's law in Equation 1.

$$A = \log\left(\frac{I_o}{I}\right) = -\log\left(\frac{1}{T}\right)$$

Where I represent light intensity at wavelength λ, I_o is intensity incident light and T depicts the transmittance. Absorption of light photons into the dyes initiate electronic activity that either causes disintegration of the dye molecules or transition to a higher energy level. Probability of absorption of a photon is directly proportional to the concentration of the dye absorber particles in the sample and length of the optical path. This is exponential of the solute

concentration where the radiation passes through a solution in accordance with Per-Lambert's law. A dual integration of both Beer Lambert and Per-Lambert's laws is given as Equation 1 [17]. The optical properties such as highest occupied molecular orbital to lowest unoccupied molecular orbital (HOMO–LUMO) energy gaps of π-conjugated dye systems were evaluated as shown in Figure 2. The optical frequency bandgap values are 3.6 eV, 3.5 eV, 0.75 eV and 0.5 eV for Butternut, Neem, Beetroot and African Star Apple respectively.

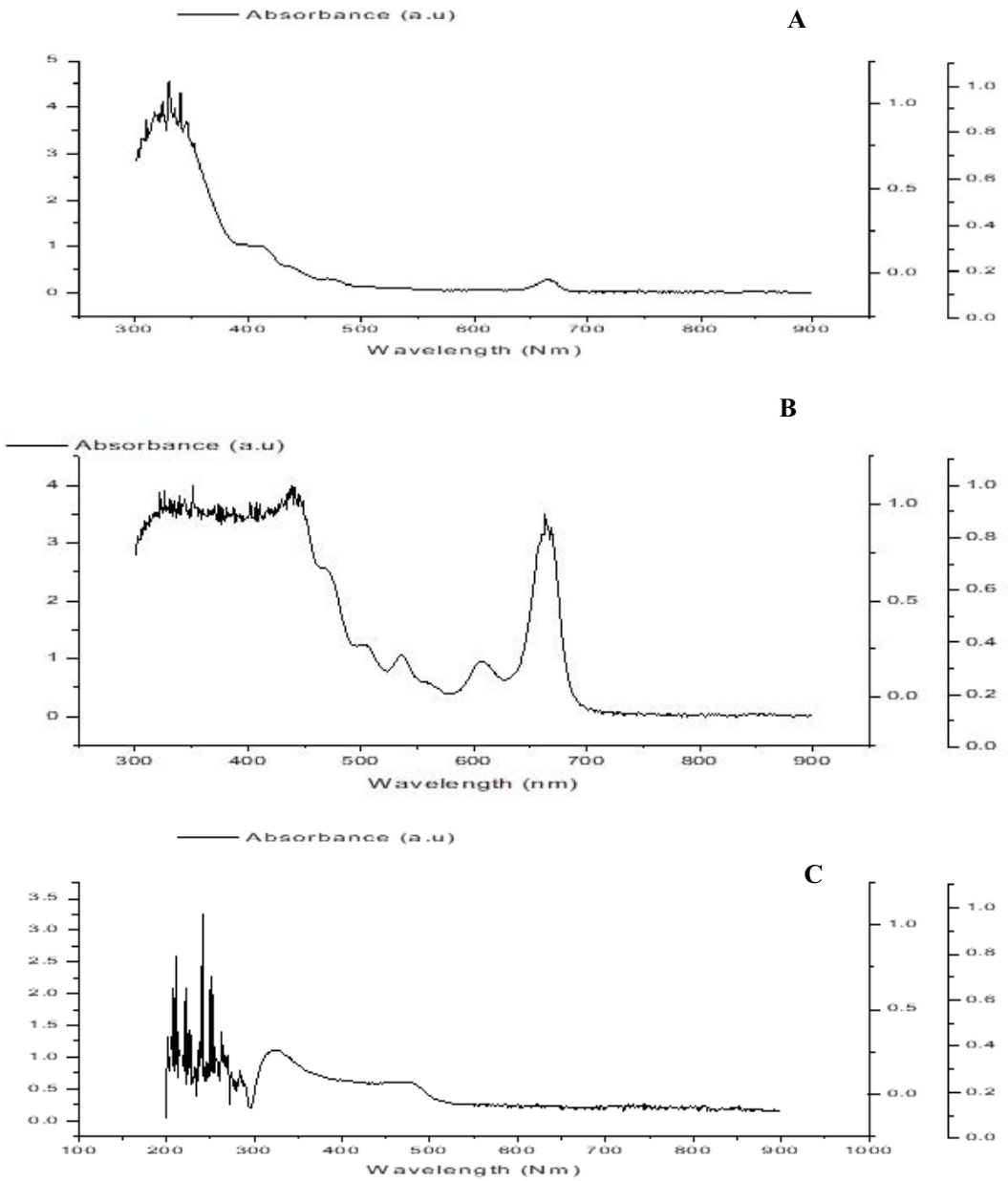

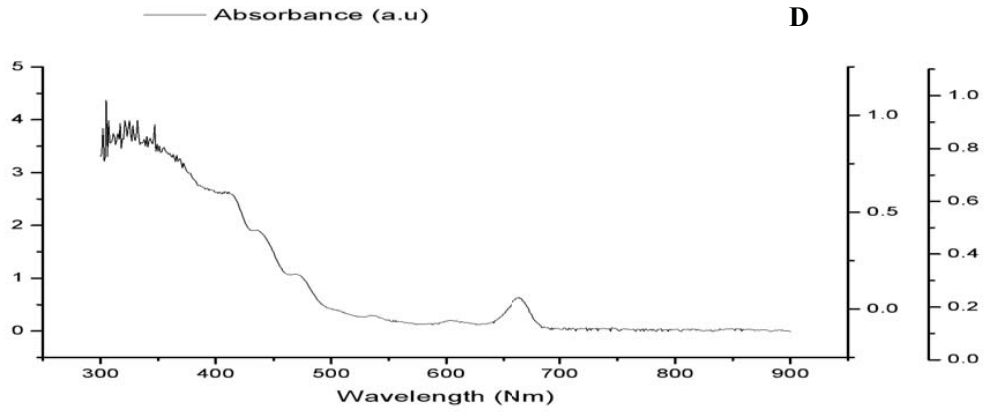

Figure 1: UV/Vis Spectrographs of (A) Butternut (B) Neem (C) Beetroot (D) African Star Apple

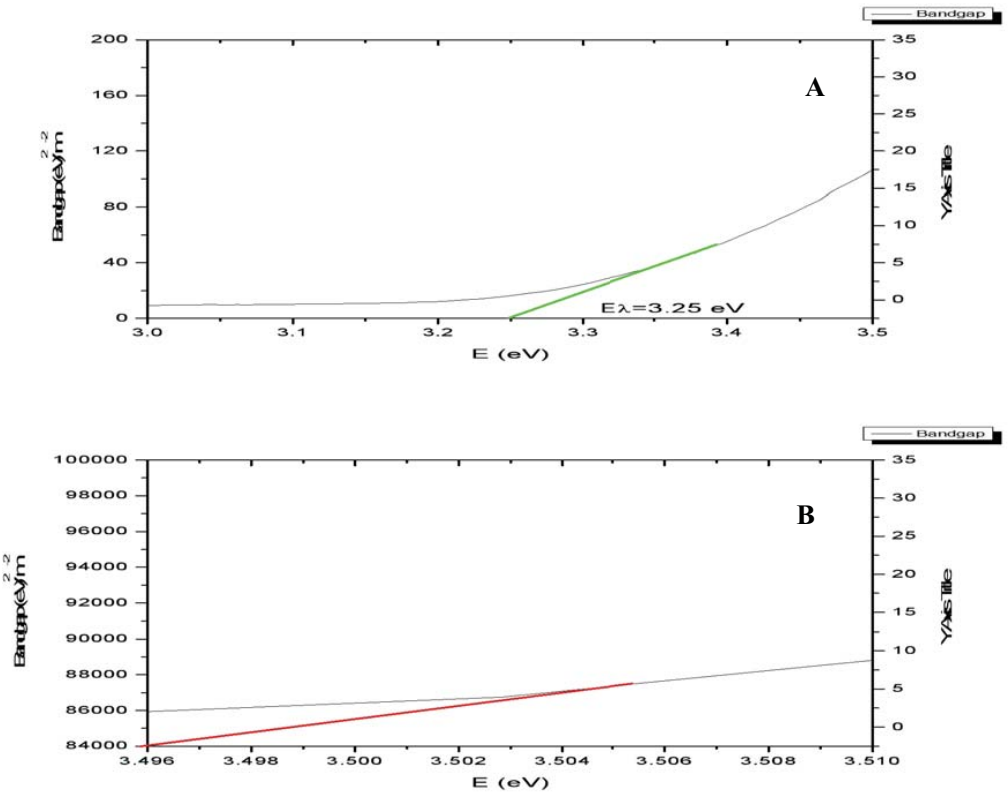

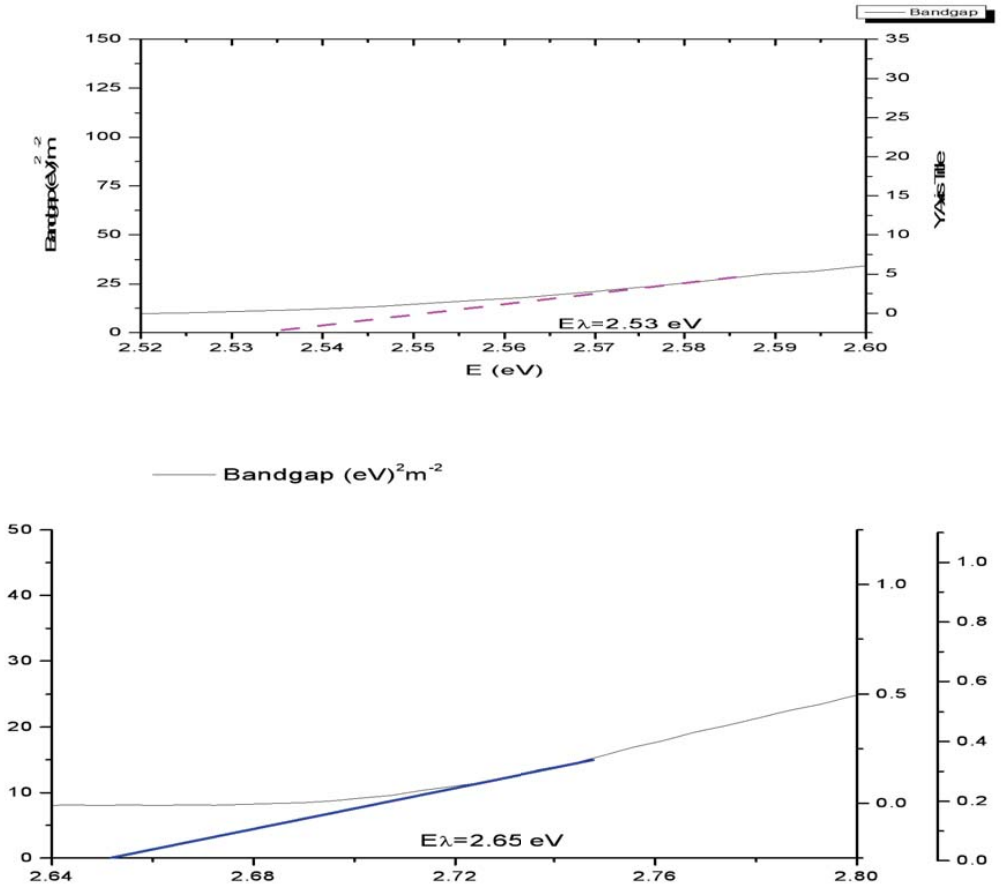

Figure 2: Determination of Bandgap of (A) Butternut (B) Beetroot (C) Neem (D) African Star Apple (ASA)

The difference between the photonic bandgap responsible for the HOMO to LUMO electronic jumps and the UV/Vis determined bandgap is as presented on Table 1. LUMO-HOMO jump is consequent of quanta of photons absorbed from electromagnetic radiation, butternut chromophores made the highest transition equivalent to 3.6 eV. The lowest transition occurred in ASA with energy transition equivalent of 0.5 eV. Neem transits within the range same range as Butternut while, Beetroot transits close to an energy range of ASA. The optical frequency bandgap determined from the UV/Vis spectrographs of the four dyes records a threshold value in Beetroot with a large value of ≈3.5 eV. The least value was observed in Neem with a value of 2.5 eV. This range corroborates the usual bandgap range for semiconductors from existing records. Interpretation of the semiconductor bandgap range (x-

axis) by tracing the equivalent direct bandgap for the dye extracts gives a sharp contrast between the least and threshold value. Neem and Butternut direct bandgaps occur within the same range, the least is ASA. An abnormally high direct bandgap was observed in Beetroot with a value of 84,110.98 eV. This will be explained later using their elemental composition and electron conductivity quotient.

Table 1: Comparison of HOMO-LUMO Bandgaps with UV/Vis determined Bandgaps.

Dye Extract	Photonic Bandgap (eV)	Optical frequency Bandgap (eV)	Mean Direct bandgap for semiconductor (eV)
Butternut	3.60	3.247	0.64
Beetroot	0.75	3.496	84110.98
Neem	3.50	2.534	0.48
African Star Apple	0.50	2.651	0.11

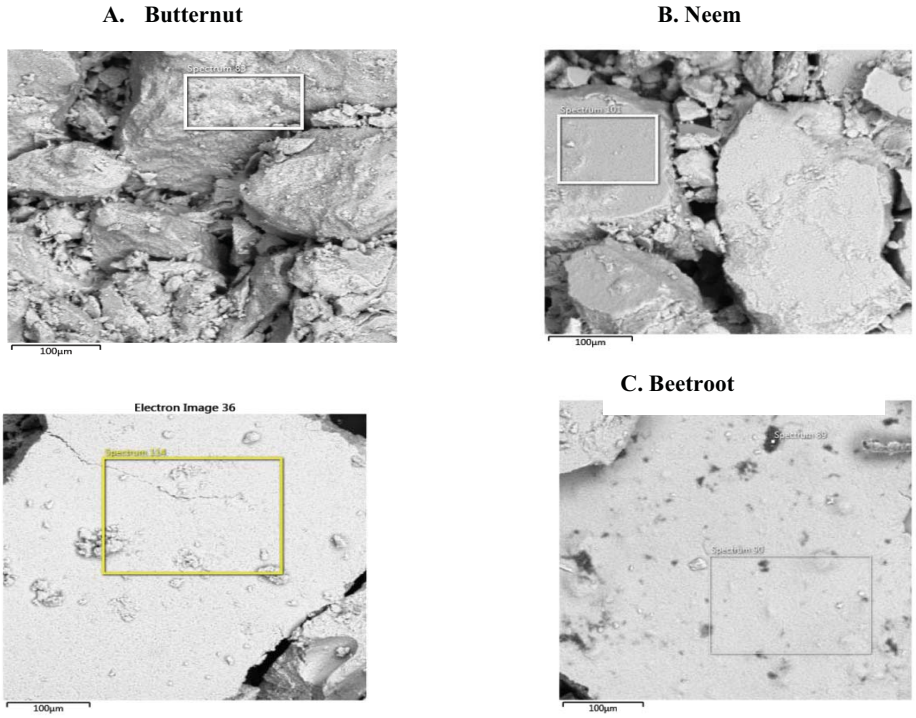

Figure 3: Scanning Electron Microscopy of the dye topography at the surface

Scanning Electron Microscopy: The surface of each dye microstructure is as revealed in Figure 3, at a high resolution of 100 µm. In spite of dissolution of the dye culture in solvent, different grain boundaries are observed which is responsible for the property exhibited or

characteristic of the nanomaterials when applied. Butternut and Neem show multivariate grain boundaries while Beetroot and ASA reveal particulate grain boundary. The overall effect is a coarse surface in both Butternut and Neem although, there is more interconnectivity between the butternut microparticles. Neem shows gaps which would eventually act as trap sites. Beetroot shows uniformity and good interlocking between neighbouring particles, but for small fringes at the peripheral, the cross-section is near perfect. ASA is dotted sporadically with tiny black dots where the microparticles experience discontinuity, these pose recombination risks during charge transport. All EDS of the four extracts record a high presence of Titanium oxide owing to the photoanode frame, ASA reveals a rich nanocomposite as shown in Figure 4.

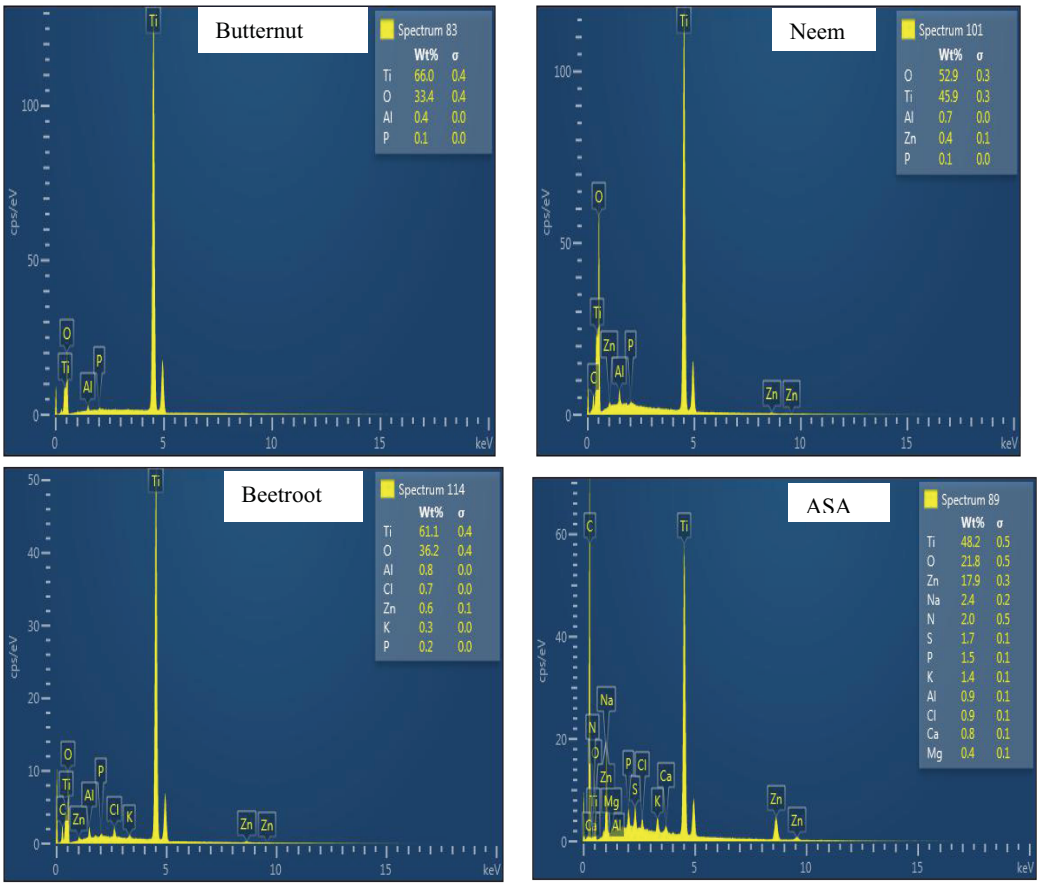

Figure 4: Energy dispersive spectrum of the dye extracts

Electron conductivity of organic extracts: Charge transport across the surface topography of these four extracts is quite diverse as indicated using Gwydion software in Figure 5. The red dots illustrate electron seats where electrons hop from one spot to another through diffusion. The blue zones represent regions that favour electron tunnelling, considering this area relative to the earlier discussed photonic bandgap and direct semiconductor bandgap, Neem has a prominent trap site at the centre of its cross-section, charge transport will be greatly impeded.

In Butternut, the electron seats are not closely packed, the energy absorbed from the photons is ≤ bandgap so most occupy the middle level in the valence band. The myriad of elemental particles in ASA as shown in Figure 4 (D) aid electron conductivity, this accounts for the high density of electron seats at the higher energy level in Figure 5 (D). In Beetroot, the highest optical frequency shown is bridged by the second-best elemental composition, this facilitate energetic hops comparable to the width of the blue region. Electrostatic potential build-up is high due to the closely packed electron seats, the effect is the remarkable semiconductor direct band gap shown in Table 1.

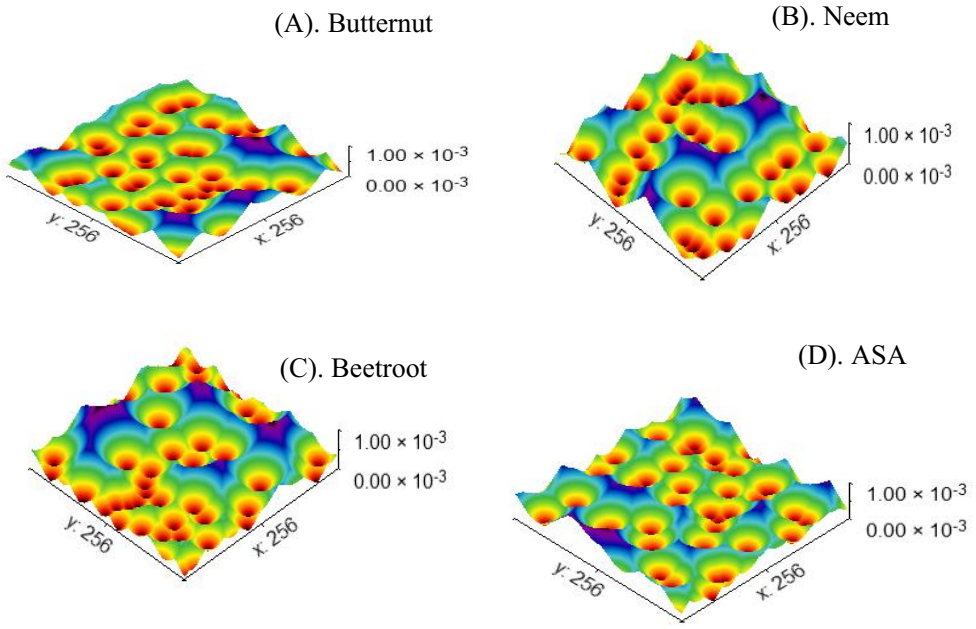

Figure 5: Electron Conductivity spectroscopy of four organic extracts with Gwydion software

Mean Estimate of Conductivity across surface topography of Organic Extracts: A further assessment of carrier density on the surface of each dye using Gwydion software is illustrated in Figure 6 corroborates Figure 5. The trajectory of ASA was the most-short lived probably due to the presence of Cl, S and N in its composition, and it was characterized by a gradual transition which is quite uniform. Neem begins with florescence and successive electrons hops occur in its mid-section and a major transition at x = 0.35 mm to the upper energy level. In Butternut, there are series of electron transitions from its midsection all the way to the peak. Then a sudden florescence occurs at x = 0.85 mm, followed and sustained by a transition to the middle section.

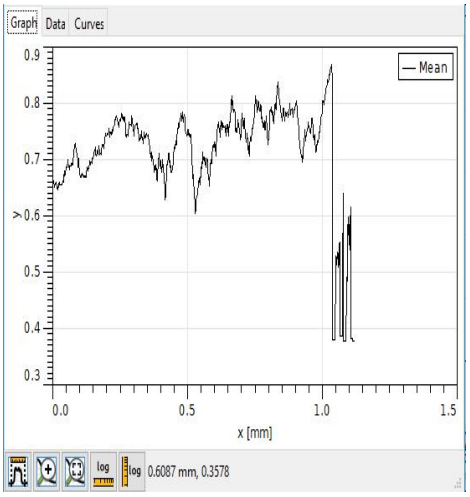
Graph
Data
Curves
Mean
0.9
0.8
0.7
y 0.6
0.5
0.4
0.3
0.0
0.5
1.0
1.5
x [mm]
log
log
0.6087 mm, 0.3578

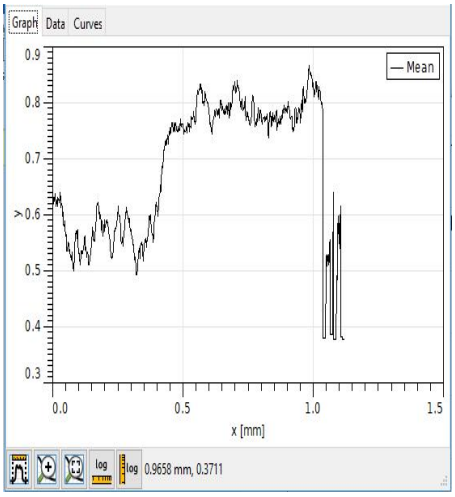
Graph
Data
Curves
Mean
0.9
0.8
0.7
y 0.6
0.5
0.4
0.3
0.0
0.5
1.0
1.5
x [mm]
log
log
0.9658 mm, 0.3711

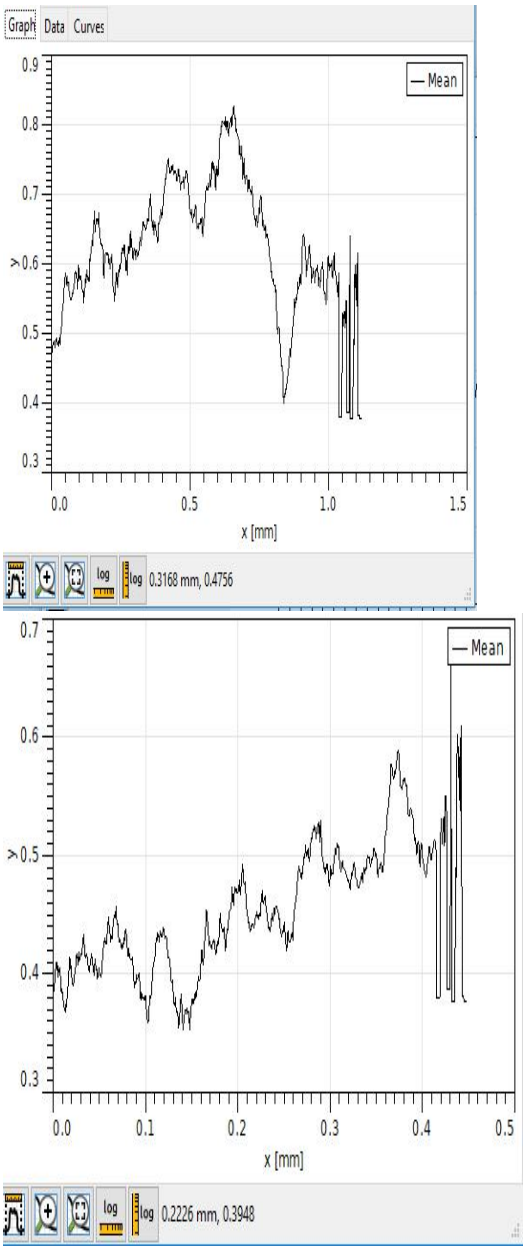

Figure 6: Mean of Charge Carrier Transport in Organic Extracts

Conclusions

There is no instant where signals at two different wavelengths interfere within the nanomaterial. The outcome of this study reveals that the band-gap energy of organic π-conjugated semiconductors is correlates with their electronic band structure. Knowledge of the band gap plays a key role, influencing the electrical conductivity of a solid. An optical power meter is recommended for further research on this present output. Control of optical frequency

energy gap in π-conjugated systems, is a very serious task for semiconductor and nanomaterial industries. Frequency is vital for communication, optical frequency is the oscillation frequency of the corresponding electromagnetic wave, which is determined by the vacuum velocity of light divided by the vacuum wavelength i.e. $\nu = c / \lambda$.

Acknowledgements
The authors wish to acknowledge the financial support offered by Covenant University in actualization of this research work for publication

Reference

[1] Qu, H., Li, J., Skorobogatiy, M. (2015). Photonic bandgap fibers—a roadway to all-fiber refractometer systems for monitoring of liquid analytes. Optofluidics, Sensors and Actuators in Microstructured Optical Fibers, 247-283.
[2] Akhtar, J., Aamir, M., Sher, M. (2018). Organometal Lead Halide Perovskite. Perovskite Photovoltaics. Basic to Advanced Concepts and Implementation, 25-42.
[3] Smith, A. M. and Nie, S. (2010). Semiconductor Nanocrystals: Structure, Properties, and Band Gap Engineering. Acc. Chem. Res., 43(2): 190–200.
[4] Van mullekomj, H. A. M., Vekemanse, A. J. M. Havinga, E., Meijer, W. (2001). Developments in the chemistry and band gap engineering of donor–acceptor substituted conjugated polymers. Materials Science and Engineering: R: Reports, 32 (1), 1-40.
[5] Sitt, A., Hadar, I., Banin, U. (2013). Band-gap engineering, optoelectronic properties and applications of colloidal heterostructured semiconductor nanorods. Nano Today, 8, (5), 494-513.
[6] Krahne, R., Morello, G., Figuerola, A., George, C., Deka, S. L. (2011). Advanced Environmental Analysis: Applications of Nanomaterials, Phys. Rep., 501 (2), 75-221.
[7] Deutsch, Z., Schwartz, O., Tenne, R., Popovitz-Biro, R., Oron, D. (2012). Efficient exciton concentrators built from colloidal core/crown CdSe/CdS semiconductor nanoplatelets. ACS Nano Letters, 14 (3): 1559–1566.
[8] Jain, P. K., Beberwyck, B. J., Fong, L., Polking, M. J., Alivisatos, A. P. (2012). Highly luminescent nanocrystals from removal of impurity. Angew. Chem.Int. Ed., 51(10), 2387-2390.
[9] Hadar, I., Hitin, G. B., Sitt, A., Faust, A., Banin, U. (2013). Band-gap engineering, optoelectronic properties and applications of colloidal heterostructured semiconductor nanorods. J. Phys. Chem. Lett., 4, 502-507.
[10] Al-Hussainey, A. M. and Abbas, T. M. (2018). Study the Optical and Spectral Properties of Organic Dye as an Effective Medium in Dye Lasers. Journal of Global Pharma Technology, 10(5), 304-311.
[11] Bouit, P-A., Guillaume, W., Feneyrou, P., Bretonnière, Y., Kamada, K., Maury, O., Andraud, C. (2008). Near IR two photon absorption of cyanines dyes: application to optical power limiting at telecommunication wavelengths. Proceedings of SPIE: The International Society for Optical Engineering

[12] Huo, F., Zhang, H., Chen, Z., Qiu, L., Liu, J., Bo, S., Kityk, I. V. (2019). Novel nonlinear optical push–pull fluorene dyes chromophore as promising materials for telecommunications. J Mater Sci: Mater Electron, 30, 12180–12185.
[13] Nikolaev, S. V., Pozhar, V. V., Dzyubenko, M. I., Nikolaev, K. S. (2018). Dependence of fluorescent characteristics of nanocomposites on the basis of dye molecules and silver nanoparticles on the optical density of components. Telecommunications and Radio Engineering, 77 (19).
[14] Abodunrin, T. J., Boyo, A.O., Usikalu, M.R. (2018). Data on the porphyrin effect and influence of dopant ions on Thaumatococcus daniellii dye as sensitizer in dye-sensitized solar cells. Data in brief, 20, 2020-2026.
[15] Abodunrin, T., Boyo, A., Usikalu, M., Obafemi, L., Oladapo, O., Kotsedi, L., Yenus, Z., Maaza, M. (2017). Microstructure characterization of onion (A. cepa) peels and thin films for dye sensitized solar cells. Materials Research Express, 4 (3), 035503.
[16] Pascal, S., Bellier, Q., David, S., Bouit, P-A., Chi, S-H., Makarov, N. S., Guennic, B. L., Chibani, S., Berginc, G., Feneyrou, P., Jacquemin, D., Perry, J. W., Maury, O., Andraud, C. (2019). Unraveling the Two-Photon and Excited-State Absorptions of Aza-BODIPY Dyes for Optical Power Limiting in the SWIR Band. The Journal of Physical Chemistry C**,** 123 (38), 23661-23673.
[17] Sulochana, B., Archana, B., Bhagwat, A., Sekar, N. (2020). Orange-Red Fluorescent (Partially Rigidified) Donor-π-(rigidified)-Acceptor System – Computational Studies. Journal of Fluorescence**,** 30 (3), 565-579.